Sediment deformation atop the Lomonosov Ridge, central Arctic Ocean: Evidence for gas-charged sediment mobilization?

Yngve Kristoffersen [a,*], John K. Hall [b], Espen Harris Nilsen [c]

[a] (retired) Department of Earth Science, University of Bergen, N-5020, Bergen, Norway
[b] (retired) Geological Survey of Israel, Jerusalem, Israel
[c] Lundin Energy Norway, 1366, Lysaker, Norway

ARTICLE INFO

ABSTRACT

We have used a hovercraft platform drifting with the sea ice to acquire the first digitally recorded seismic reflection data transects across the Canada/Greenland (89°N-85°N) section of the Lomonosov Ridge, central Arctic Ocean. The flat-lying, laterally uniform Cenozoic sediment package on top of the ridge at 87°N, 60° W shows at least four sites with local seismic amplitude anomalies. The common feature is a column (<600 m wide) of partly discontinuous or chaotic bright reflection events at the center of a <1.5 km wide dome (amplitude <25 m) terminating at the seabed in a 8–12 m deep depression. The amplitude anomalies are interpreted as gas-charged fluid escape pipes marked by a pockmark at the seabed. Gas and fluids introduced from below have mobilized the overlying high porosity, low density Eocene bio-siliceous ooze causing the doming. The gas and fluids appear to originate from the top of rotated fault blocks and sub-basalt sediments of Mesozoic or older age deposited when the Lomonosov Ridge was part of the pre-Late Cretaceous continental margin north of Franz Josef Land.

1. Introduction

The Lomonosov Ridge is an 1800 km long and 150–200 km wide continental sliver which divides the Arctic Ocean into an old (Late Cretaceous and older) basin between the North Pole and Alaska, and a younger Late Cretaceous/Cenozoic basin between the North Pole and Svalbard/Franz Josef Land (Fig. 1). The dimensions of the ridge exceed those of the Alps in central Europe as the flat top is elevated up to 3 km above the flanking abyssal plains.

The Canada/Greenland side (89° N- 85° N) of the Lomonosov Ridge is below the broad stream of old heavily ridged sea ice flowing out of the Arctic Ocean (Rigor et al., 2002) and is only accessible for seismic profiling from drifting ice stations. The exception is a 10 km long multichannel seismic section acquired by icebreaker (Knudsen et al., 2017) across the ridge perimeter at 89° N (Fig. 1, green track). As a result, the only seismic transects available across the level top of the ridge are a single drift track collected in 1965 from the ice drift station *Arlis II* using a five kilo-watt sparker recording on electrostatic paper (Ostenso and Wold, 1977) and three traverses made in 1985 by the Soviet ice station *North Pole -28* (Fig. 1, red track). The seismic source used on *North Pole-28* (NP-28) was blasting caps fired at 500 m intervals

(Gramberg et al., 1991; Langinen et al., 2009). The signals were recorded on analog tape and later digitized. The first ridge transects between 89° N and 85° N producing modern seismic data (Fig. 1, white tracks) are three complete and one partial crossings obtained during the *Fram-2014/15* ice drift (Kristoffersen et al., 2016). This was single channel seismic data from a 0.3-L air gun source digitally recorded at 25 m shot spacings. Here, we report on four crestal sites showing local seismic amplitude anomalies forming wide pipes flanked by up-bent layering. We suggest an origin related to gas-charged fluid migration from deeper pre-Cenozoic hydrocarbon source rocks.

2. Geological setting

The Alaska-facing side of the Lomonosov Ridge (Fig. 1) represents the continental margin between Greenland and west Siberia in the pre-Cenozoic Arctic Ocean (Blakey, 2020). The Lomonosov Ridge was rifted off the continental margin of Mesozoic polar Europe as the North Atlantic mid-ocean ridge system propagated into the Arctic Ocean during the Paleocene (Wilson, 1963; Johnson and Heezen, 1967, Karasik, 1968; Vogt et al., 1979, Glebovsky et al., 2006; Moran et al., 2006). The Lomonosov Ridge appears aseismic within the time span covered by the
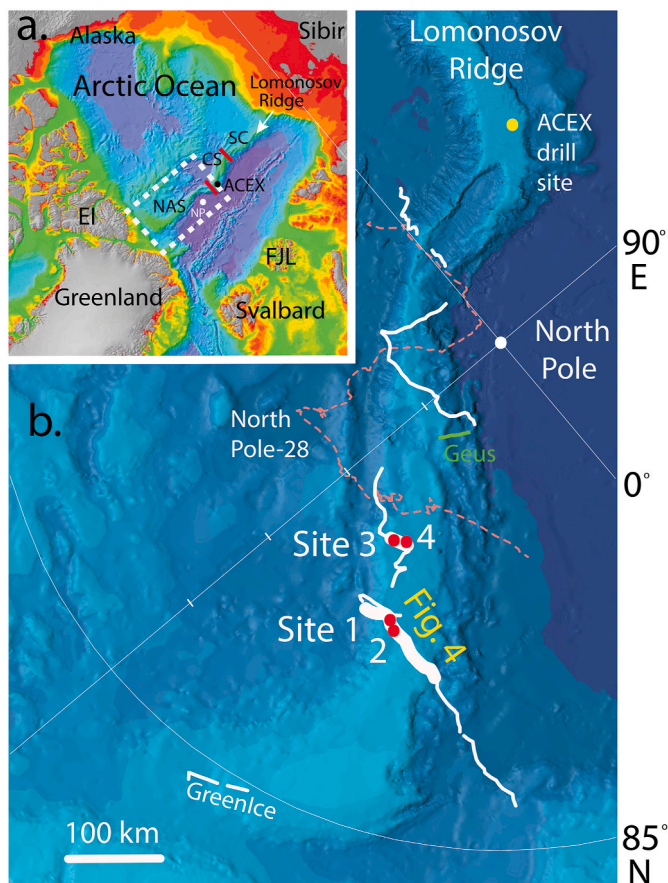

Fig. 1. a. The bathymetry of the Arctic Ocean with study area on the Lomonosov Ridge marked by white dashed rectangle (Jakobsson et al., 2012). The ridge may be divided into three segments and the boundaries between the Siberian- (SS), the Central- (CS) and the North American (NAS) segments are marked by short red bars (Rekant et al., 2019). b. Location of sites 1–4 (red dots) and the ACEX drill site (yellow dot) on the Lomonosov Ridge in the central Arctic Ocean. The drift tracks of ice station *Fram-2014/15* (thin white lines) and line drawings of the seismic sections shown in Fig. 4 are indicated by heavy white lines. Other ice drift seismic reflection profiles are from *North Pole-28* (red dashed track, Langinen et al., 2009) and *Project GreenIce* (white line, Kristoffersen and Mikkelsen, 2006). A multichannel seismic reflection profile (*Geus*, green line) acquired by icebreaker is from Knudsen et al. (2017) and the IBCAO base map from Jakobsson et al. (2012). . (For interpretation of the references to colour in this figure legend, the reader is referred to the Web version of this article.)

instrumental record (http://nnsn.geo.uib.no/intaros_eqcat/), with the exception of a possible submarine volcanic eruption experienced by the Soviet ice drift station *North Pole 3* in 1956 (Gakkel, 1958).

The Lomonosov Ridge may be divided into three segments (Fig. 1, insert) based on its morphology and the tectonic trends of its internal crustal blocks (Rekant et al., 2019). The Siberian segment is formed by numerous narrow parallel blocks and the Central segment has two large slightly oblique trending parallel blocks. The North American segment is dominated by smaller blocks in the narrow part near the North Pole and a large block south of 89° N (Fig. 1). The sediment deposits on the Central segment of the ridge as studied by seismic surveys and scientific drilling (Fig. 1, ACEX site) show a Mesozoic wedge prograding towards Alaska capped by a 420 m thick flat-lying early Eocene-Recent sediment section (Jokat et al., 1992; Shipboard Scientific Party, 2005, Moran et al., 2006). The flat-lying section consists of an upper ᵛ193 m thick unit (Unit 1/1-1/4) of unconsolidated silty clay younger than late early Miocene (Fig. 2). An apparent ᵛ 26-million-year stratigraphic gap within subunit 1/5 (ᵛ6 m thick) separates the upper clays from the underlying

early Eocene dark homogeneous silty clay (Unit 1/6, 22 m thick) which overlies a ca. 93 m thick sequence (Unit 2) of bio-siliceous silty clay and ooze (Shipboard Scientific Party, 2005; Moran et al., 2006; Backman et al., 2008). This apparent stratigraphic gap could possibly represent an extended period of slow sedimentation from latest Eocene to early late Miocene (Poirier and Hillaire-Marcel, 2011; Chernykh and Krylov, 2017). The lowermost unit of silty clay to mudstone (Unit 3) extends into the earliest Eocene and rests with an angular unconformity on sandy sediments of Campanian age (Jokat et al., 1992; Backman et al., 2008).

The North American segment of the Lomonosov Ridge was studied by three seismic transects of the ice drift station *NP-28* (Fig. 1). Langinen et al. (2009) correlated the acoustic reflection pattern of the upper 0.4 s at 88° N with the Cenozoic section at the ACEX drill site. The underlying <1 s thick sediments above acoustic basement at this latitude are thickest on the Alaska-facing side of the ridge.

The post-Early Eocene history of the Lomonosov Ridge as documented by scientific drilling on the Central ridge segment, is dominated by hemipelagic sediment deposition with a contribution of fines contributed by bottom currents and coarser material brought in by sea ice (Moran et al., 2006). The hemi-pelagic section forms a uniform drape over the flat top and is tapered along the ridge perimeter over the highest part of the ridge (Jokat et al., 1992; Langinen et al., 2009) by contour-following bottom currents (Bowden, 1960; Hunkins et al., 1969; Bird et al., 1982; Rudels et al., 1999; McCave et al., 2001). Along-ridge sedimentation rates are only known for the middle to late Quaternary part and appear to vary by a factor of more than five (Nørgard Pedersen et al., 2007; Sellén et al., 2008; Polyak and Jakobsson, 2011). The sediment supply during this period was highest at the Siberian end of the Lomonosov Ridge and lowest over the end north of Canada/Greenland.

3. Materials and methods

Old and heavily ridged sea ice makes the area south of 89° N on the North American segment of the Lomonosov Ridge inaccessible for seismic surveys by icebreakers. We have used a hovercraft platform (Fig. 3) drifting with the sea ice at about 5 km/day to acquire about 1000 km of seismic reflection data (Kristoffersen et al., 2016). The data reported here was obtained in ambient temperatures between −30 °C and −43 °C during the polar night from December 2014 through February 2015. Our sound source was a single 0.3-L (20 inch³) air gun at 3 m depth below the ice powered by a diving compressor. The signal was received by a single hydrophone suspended just below the <2 m thick ice at a 25 m offset from the source and recorded at a 2 ms sampling rate (Fig. 3). The oscillations from the air bubble released by the air gun delayed by about 60 ms presented an extra challenge as the working air pressure was sometimes allowed to decay 10–20 bar below the nominal 140 bar value. Removal of the bubble pulse therefore required accurate tracking of the variation in arrival time of the pulse followed by a trial-and-error procedure to estimate its effective frequency content (Kristoffersen et al., 2021). The processing sequence includes time variable bandpass filtering (10–140 Hz), enhancement of coherent events in the tau-p domain, source deghosting and Kirchoff time migration. The dominant frequency at the seabed is ᵛ60 Hz and ᵛ40 Hz at 1 s (two-way travel time) sub-bottom depth giving a resolution (λ/4) of 8–10 m. The zero-phase data is displayed following the SEG-polarity convention. For travel time-depth conversion in the Cenozoic sediments, we use a compressional velocity of 1.6 km/s based on the results from the ACEX drill site (O'Regan et al., 2010).

4. Results

A seismic transect across the North American segment of the Lomonosov Ridge at about 87° N shows sediments onlapping the acoustic basement from the Alaska side (Figs. 1 and 4, upper panel). The total sediment thickness ranges from 0.7 s (two-way travel time) in the west to 0.2 s in the east. We first established a tentative seismic
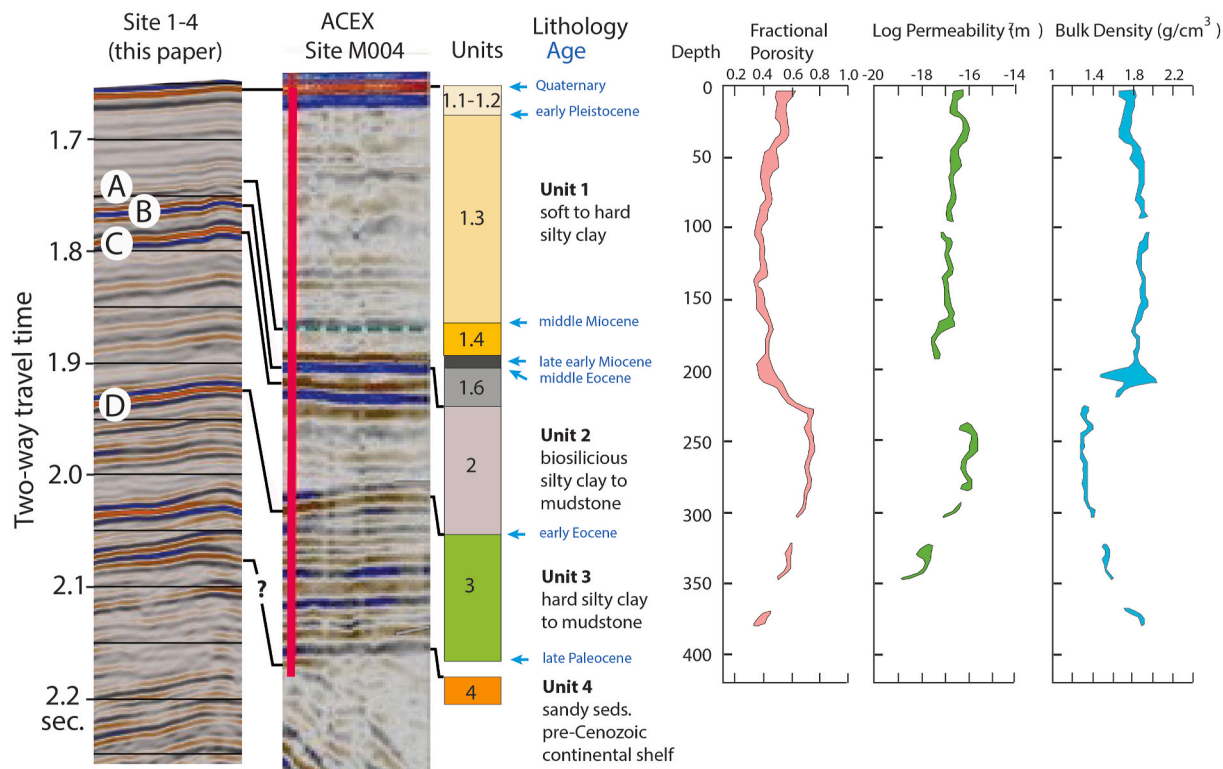
Fig. 2. Correlation of acoustic horizons between the ACEX drill site and sites 1–4. The locations of the sites are shown in Fig. 1. The lithostratigraphy is from Expedition 302 Scientists (2006), stratigraphic ages from Backman et al. (2008) and physical properties (envelope of values) are modified from O'Regan et al. (2010). Note the significantly higher porosity and decrease in bulk density of the biosilicious silty clay of Unit 2.

Fig. 3. The hovercraft ice camp (upper) with the seismic source (lower left) and the recording instruments (lower right).
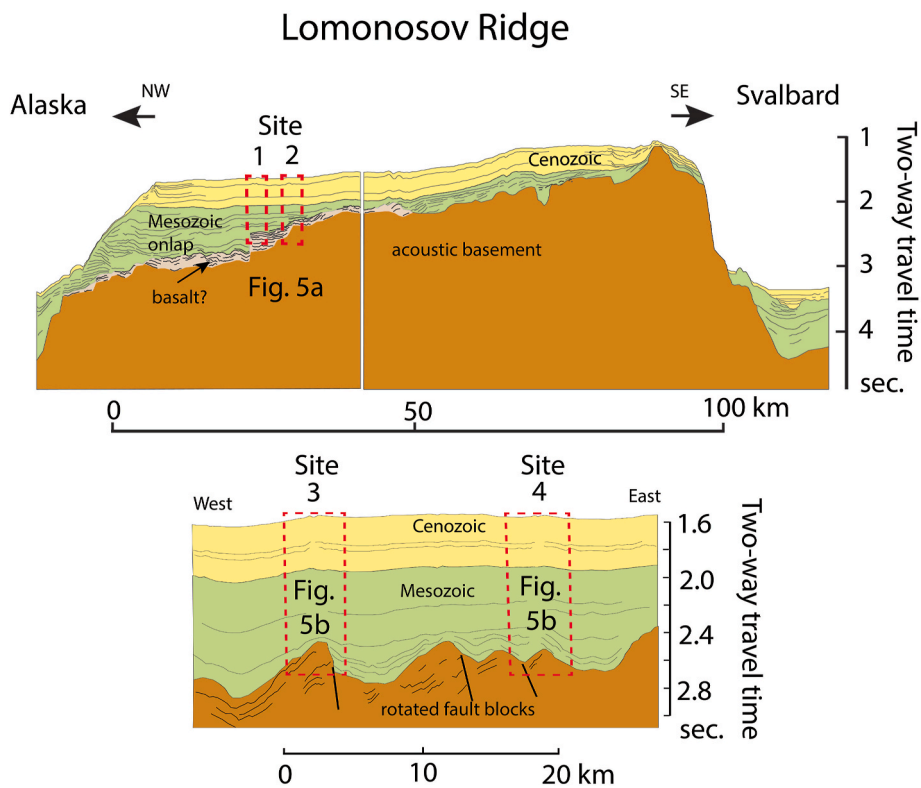
Fig. 4. Line drawing of the seismic sections over the Lomonosov Ridge with the location of sites 1–4. The locations of the seismic sections are shown by heavy white lines in Fig. 1. The stratigraphic ages are based on the correlation shown in Fig. 2.

stratigraphy by acoustic signature correlation of the undisturbed hemi-pelagic Cenozoic sediment cover on the top of Lomonosov Ridge at 87° N with the reflection sequences across the ACEX drill site (Figs. 1 and 2). The characteristic features at 87° N (Fig. 2, left column) are two close reflection events around 1.8 s (reflectors B and C) and a package of high amplitude reflectors from 1.93 s to 2.1 s. This pattern matches the reflectivity pattern across the ACEX drill site except for a much thinner

section of the soft-to-hard silty clay of Unit 1 above reflector B (Fig. 2). The correlation suggests the reverse standard polarity reflector B at 87° N corresponds to the top of the bio-silicious silty clay to mudstone (Unit 2) of ACEX. We consider reflector D to be time equivalent to the top of the silty clay Unit 3 (early late Eocene) associated with a 40–50 m thick Opal A-C/T reaction zone (Ogawa et al., 2008; O'Regan et al., 2010).

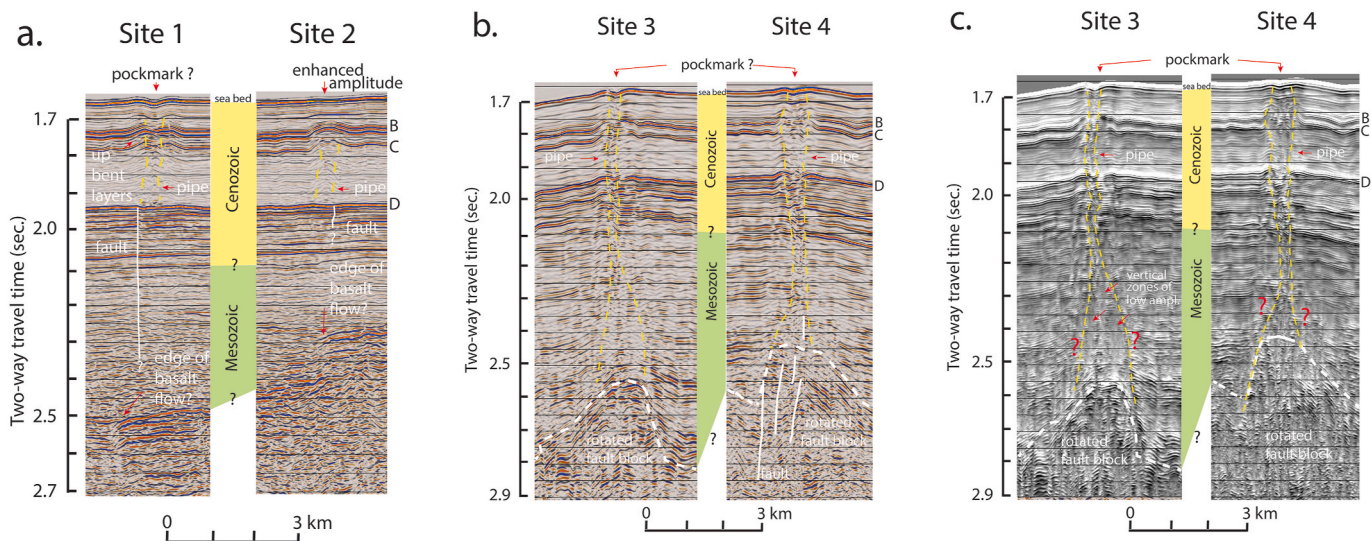The seismic data show distinct seismic amplitude anomalies below

Fig. 5. a. Migrated seismic sections across site 1 and 2. Site locations are shown in Figs. 1 and 3. The stratigraphy is from Fig. 2. Tentative outlines of the pipes are marked by dashed yellow lines. b. Migrated seismic sections across site 3 and 4. Site locations are shown in Figs. 1 and 3. The stratigraphy is from Fig. 2. Tentative outlines of the pipes are marked by dashed yellow line and the outlines of rotated fault blocks by dashed heavy white lines. c Migrated seismic sections across sites 3 and 4 displayed in grey scale with illumination from above to enhance linear vertical structures in the pipe architecture. Tentative outlines of the pipes are marked by dashed yellow lines and deep fault blocks by dashed heavy white lines. . (For interpretation of the references to colour in this figure legend, the reader is referred to the Web version of this article.)

the seabed at four separate locations (Figs. 1, 4 and 5). Sites 1 and 2 are within 5.4 km of each other. Sites 3 and 4 are separated by 15 km and Site 3 is about 150 km away from Site 1 and 2. The acoustic stratigraphy at the four sites (Figs. 5 and 6) is characterized by:

i) A ⏴ 600 m wide column of seismic amplitude anomalies centered within a <1.5 km wide zone of up-bent reflection events (Figs. 5 and 6).

ii) Short bright reflection segments of reverse standard polarity are present within the amplitude anomaly column at all sites and the columns terminate in a depression at the seabed, except at Site 2 (Figs. 5a and 6a).

iii) The up-bending starts at reflector D at sites 1 and 2 and increases slightly upwards (Fig. 6a) while up-bending at sites 3 and 4 also involves strata below reflector D (Fig. 6b).

The column of amplitude anomalies at Site 1 starts with bright reflection segments at the level of reflector D in the vicinity of a fault trace (Fig. 6a). The fault may extend down to high amplitude reflections at 2.5 s depth (Fig. 5a). These reflections appear flat over distances >3 km. The thickness of the high amplitude reflection package is 50 ms or more (>100 m assuming 4 km/s). Below sites 3 and 4, the amplitude anomaly columns are positioned directly over the crests of rotated blocks which are internally stratified (Fig. 5b and c).
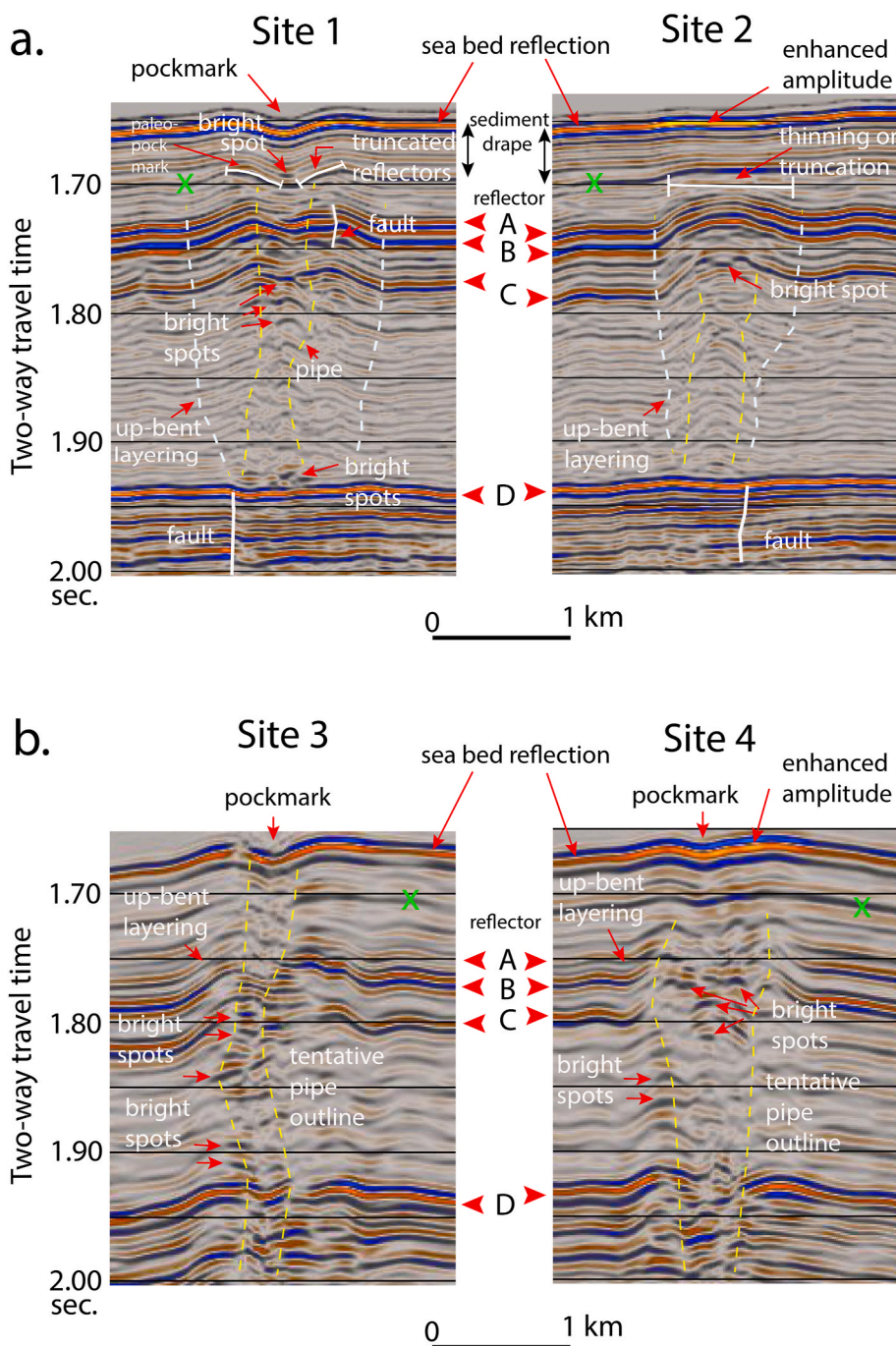

Fig. 6. a. Detail of seismic section across sites 1 and 2 with outlines of up-bent layering marked by dashed white line and pipe anomalies by dashed yellow lines. At Site 1 the truncated reflections form a paleo-pockmark. The apparent reflection event labelled X is considered an artifact from incomplete removal of the bubble pulse. b Detail of seismic section across sites 3 and 4 with outlines of the pipes marked by dashed yellow lines. The apparent reflection event labelled X is considered an artifact from incomplete removal of the bubble pulse. . (For interpretation of the references to colour in this figure legend, the reader is referred to the Web version of this article.)

5. Interpretation

5.1. The seismic amplitude anomalies

The numerous short bright reflection segments present in the columns of amplitude anomalies at sites 1–4 suggest the presence of free gas in the sediments (Løseth et al., 2009). Also, the acoustic images across sites 1–4 are similar to seismic images of stratigraphy where focused expulsion of fluids and gas has been documented (Løseth et al., 2001, 2009; Svensen et al., 2003; Hansen et al., 2005; Hansen, 2006; Judd and Hovland, 2007; Moss and Cartwright, 2010; Hustoft et al., 2010; Gay et al., 2012; Cartwright and Santamarina, 2015; Maestrelli et al., 2017). We interpret the stacked chaotic reflections forming these columns or pipes of amplitude anomalies at each site to be conduits for fluids and gas expulsion, possibly related to a fracture network (Arntsen et al., 2007; Jain and Juanes, 2009). Although hydro-fracturing is commonly cited to explain how wide pipes will form in fine-grained sediments, there is thus far no published direct evidence for *in situ* fractures in pipes as identified in the seismic data (Cartwright and Santamarina, 2015) except for rare outcrop examples (Morley, 2003; Løseth et al., 2011). The more continuous reflections at sites 1 and 2 (Fig. 6a, reflectors A and B) may have minor fractures and faults of dimensions which are unresolvable in our seismic data.

5.2. The origin of up-bent acoustic layering

Any sediment deformation from a tectonic event can be ruled out as published and unpublished seismic data from the Central and North American segments of the Lomonosov Ridge show no evidence of local horizontal tectonic deformation within the Cenozoic sediment section beneath the level top of the ridge (Jokat et al., 1992; Jokat, 2005; Langinen et al., 2009; Sauermilch et al., 2018; Rekant et al., 2019; Weigelt et al., 2020). Our single channel vertical incidence seismic reflection data provide no velocity information and no offset range to facilitate attribute analysis. The apparent up-bent acoustic layering at all sites could be a velocity effect (pull-up), sediment deformation or both. These effects are discussed below.

i) velocity:

Higher velocities could derive from the presence of methane-derived authigenic carbonates and/or hydrates. Authigenic carbonate form near the sediment-water interface sourced by methane-rich fluids, but carbonate lumps and pavements associated with pockmarks may not be resolved by conventional seismic reflection data (Hovland et al., 1987; Judd and Hovland, 2007; Magalhãesa et al., 2012; Judd et al., 2020; Kravchishina et al., 2021). The syn-depositional process of carbonate production from methane is unlikely to contribute to the velocity anomalies at sites 1–4. It would require local methane input throughout deposition of the siliclastic Unit 1 and the mud-bearing siliceous oozes of Unit 2.

Gas hydrates in the sediments can increase the compressional velocity by 1 km/s or more depending on the degree of hydrate saturation (Lee et al., 1993; Guerin and Goldberg, 2005; Madof, 2018). The apparent up-bending of layers at sites 1–4 could be a velocity anomaly related to emplacement of hydrates in veins or fractures generated by gas overpressure. This has been suggested for the well-surveyed CNE03 chimney below the Nyegga pockmark field on the southeastern Vøring Plateau (Westbrook et al., 2008; Plaza-Faverola et al., 2010). The presence of hydrate was inferred from a high-velocity (up to +0.3 km/s) region in the upper 250 m below the seabed. The magnitude of the apparent up-bending at CNE03 is 50% higher than at sites 1–4 on the Lomonosov Ridge.

Gas hydrates may be inferred from the presence of a bottom simulating reflector (BSR) or reduced seismic amplitudes (Shipley et al., 1979; Lee and Dillon, 2001; Hornbach et al., 2003). There is no credible

evidence of a BSR at the predicted depth of 0.2 s below the seabed on the Central and Siberian segment of the Lomonosov Ridge (Jokat, 2005; O'Regan and Moran, 2010; Weigelt et al., 2020). This depth corresponds to that midway between reflectors C and D (Figs. 2 and 6). On the North American segment of the Lomonosov Ridge, the four crossings (Fig. 1) acquired during the *Fram-2014/15* ice drift (Kristoffersen et al., 2016) have been scrutinized for indications of a BSR reflection cross-cutting the tapered sediment strata at the ridge perimeter (Shipley et al., 1979; Berndt et al., 2004). No such indications were found. Amplitude blanking, another common characteristic of free gas above hydrate-bearing sediments (Shipley et al., 1979), is also not observed in the area of sites 1–4. However, the absence of a BSR does not necessarily mean methane is absent (Xu and Ruppel, 1999). Formation of hydrates and a BSR requires a supply of gas exceeding the solubility in seawater and losses due to diffusion and the sulphate reduction process (Zatsepina and Buffett, 1997; Borowski et al., 1999). We infer that any gas hydrate concentration is low and the effect on the compressional wave velocity at sites 1–4, is too small to explain the sediment deformation as a velocity pull-up.

ii) Sediment deformation:

The up-bent layering at sites 1–4 could also indicate the presence of mobilized sediments as suggested for the upward convex mound structures observed on the Gjallar Ridge, offshore mid-Norway (Hansen et al., 2005). The type A and B mounds on the Gjallar Ridge (Fig. 11 and 13 in Hansen et al., 2005) are interpreted to have formed by forceful upward migration of a mobilized clay-rich ooze-fluid mix driven in part by the buoyancy of exsolved gas. The mounds on Gjallar Ridge have no clear evidence of rim-synclines as is also the case on the Lomonosov Ridge (Fig. 6).

The Cenozoic section on top of the Lomonosov Ridge appears undisturbed, but includes a unit of Eocene bio-silicious ooze (Unit 2) of reduced stability (Kristoffersen et al., 2007; O'Regan et al., 2010). The up-doming at sites 1 and 2 starts at reflector D, equivalent to the base of the high porosity and low-density bio-silicious silty clay and mudstone of Unit 2. This strongly suggests the up-doming was driven by sediment mobilization within this unit (Figs. 2 and 6a). The inferred trigger was pressure induced by fluids and gas from a deeper hydrocarbon source (Fig. 5). At sites 3 and 4, the doming starts slightly deeper than reflector D and the column of amplitude anomalies extend down to the top of rotated fault blocks which may indicate pipe formation at higher pressures and supply rates of fluids and gas (Fig. 5b and c).

6. Discussion

6.1. The physical properties and stability of the cenozoic sediment section

Using the stratigraphic framework proposed in Fig. 2, we consider the observed sediment properties at the ACEX drill site (O'Regan et al., 2010) as an approximation for the condition at the sites of our seismic amplitude anomalies (Figs. 1, 2, 4–6). Based on consolidation and shear strength measurements on the drilled core material, those authors concluded that the Cenozoic section is in a state of under-consolidation or over-pressure despite low sedimentation rates. Furthermore, their one-dimensional compaction modelling suggests the overpressure is supported by fluids in excess of the estimated contribution from mechanical compaction or liberated by Opal A-C/T transformation (O'Regan et al., 2010). Thus, the flat-lying Cenozoic section at the top of the Lomonosov Ridge is in a state pre-conditioned for pipe formation or sediment mobilization driven by gas-charged fluid migration (Huuse et al., 2010). In particular, the stability of the bio-silicious ooze of the Eocene Unit 2 is reduced; its density is ∿0.4 g cm^3 lower than the overlying sediments, the porosity is high (40–60%) and the permeability is low in the lower part of the unit (Fig. 2). In this respect, the sediments share physical property characteristics with the mud rocks of the

Hordaland Group in the North Sea or the Brygge Formation off mid-Norway where evidence of extensive sediment mobilization has been observed (Løseth et al., 2003; Hansen et al., 2005).

6.2. Pipe architecture

The bright reflection segments indicate the presence of gas-charged sediments (Fig. 6). The mode of gas migration through sediments is to a large extent controlled by grain size and fracturing would be the dominant process in clays and mudstone (Jain and Juanes, 2009). Fracture networks would develop in the fine-grained hemi-pelagic Cenozoic sediments on the Lomonosov Ridge and collectively form pathways to the seabed in response to gas overpressure introduced from below. The anomalous seismic amplitude patterns at sites 3 and 4 are more chaotic throughout the length of the pipes than at sites 1 and 2. This suggests the extent of the fracture networks along with the distribution of gas and hence the compressional velocity distribution is more complex (Arntsen et al., 2007). A grey-scale plot with trace amplitudes illuminated from above enhance subtle trace-to-trace vertical low amplitude trends which may be interpreted as anastomosing pathways of the internal pipe architecture (Fig. 5c). The pipes appear to be slightly wider at the base (Fig. 5c, yellow dashed outline).

6.3. The timing of fluid and gas expulsion

Seabed pock marks are considered diagnostic of blow-out event(s) (Løseth et al., 2001, 2011, Hovland et al., 2002). Each amplitude anomaly pipe at sites 3 and 4 extends to a seabed depression interpreted as a pockmark (Fig. 6b). The mobilized sediments involve the entire stratigraphic column suggesting long term gas leakage until recent times particularly at Site 3 (Fig. 6b). At Site 1, truncated reflectors below a drape ~37 ms (~30 m) thick frame a paleo-pock mark (Fig. 6a). Later gas leakage into the drape is indicated by a small bright spot within the

drape just above the center of the truncated level. The drape covering the blow-out event(s) may have been deposited in <4 million years as the average Pleistocene sedimentation rate was 1.17 cm/ka for the central part of the Lomonosov Ridge (O'Regan et al., 2008) and 0.75 cm/ka at the Canadian end of the ridge during the late Quaternary (Nørgaard-Pedersen et al., 2007). At Site 2, the signal amplitude of the seabed reflection is enhanced, suggesting gas leakage until recent times (Fig. 6a).

6.4. Possible sources of the deep fluids and gas

The Eocene sediments recovered at the ACEX site (units 1/6, 2 and 3) had a content of total organic matter (TOC) in the range of 1–5% of algae-type origin accumulated under anoxic-euxinic conditions (Stein et al., 2006; Stein, 2007). However, the low overburden (~200 m) has resulted in a state of thermal maturity insufficient for hydrocarbon generation (Mann et al., 2009). Therefore, possible source rocks for the gas have to be the underlying Mesozoic or older stratigraphic levels (Moore et al., 2011).

At site 1, the gas-charged sediments above reflector D appear to be connected to high amplitude reflections at 2.5 s depth via a fault (Fig. 5a). The reflections are interpreted as the distal ends of lava flows as they lack cusp-like terminations characteristic of intrusions (Malthe-Sørensen et al., 2004; Planke et al., 2005). Permeability anomalies associated with the fault may have allowed fluids and gas from over-pressured sub-basalt hydrocarbon sources to escape to the seabed at Site 1. The communication between the pipe at Site 2 and a source region at depth is less clear (Fig. 5a). At sites 3 and 4, the pipes are located directly above rotated stratified fault blocks (Fig. 5b and c). We suggest that these fluid and gas expulsion pipes at sites 3 and 4 have been sourced from hydrocarbon reservoir(s) with a connection to their respective fault blocks.

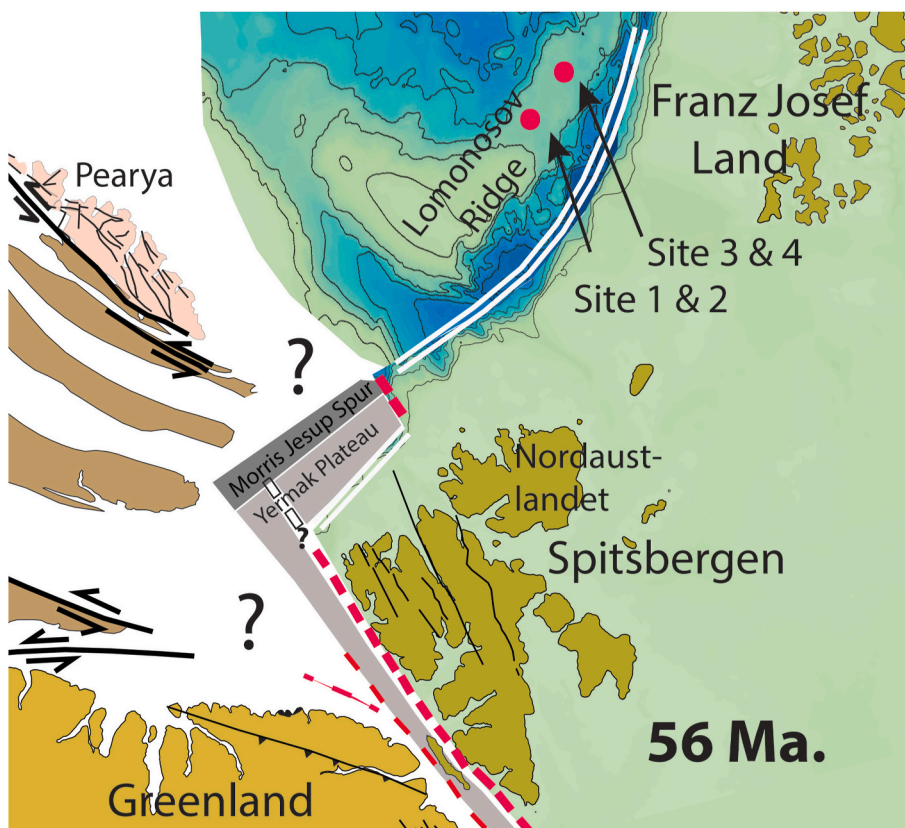The paleo-position of sites 1–4 was north of Franz Josef Land prior to

Fig. 7. Reconstruction of the position of sites 1–4 relative to Europe (Franz Josef Land) at the time of initiation of seafloor spreading in the Eurasia Basin using GPlates software (www.earthbyte.org). Figure modified from Kristoffersen et al. (2021). Europe (Svalbard) is fixed and the Eurasia Basin closed using rotation parameters from Gaina et al. (2002) and the relative position of Greenland restored using parameters from Barnett-Moore et al. (2016). The crustal fragments north of Greenland are adapted from Piepjohn et al. (2016).

Late Cretaceous rifting and opening of the Eurasia Basin during the Cenozoic (Fig. 7). An up-to 500 m thick section of basalt flows with interbedded tuffs, sandstones, shales and siltstone of Hauterivian to Albian age (130-100 Ma) is present on Franz Josef Land (Dibner, 1978, 1998; Campsie et al., 1988; Corfu et al., 2013; Shipilov, 2016). The volcanics are considered to be part of a larger High Arctic Large Igneous Province (HALIP) (Buchanan and Ernst, 2006; Drachev and Saunders, 2006) which we assume may also include the basalts on Lomonosov Ridge being the continental margin to the north at that time (Fig. 7). If so, the primary source of fluids or gas which mobilized the shallow sediments at sites 1–4 were beds of possibly Early Cretaceous age or older. At that time, the Arctic Ocean was a closed basin with restricted connections to the global ocean (Zakharov et al., 2011; Akhmetiev et al., 2012; Schroder-Adams, 2013; Brikiatis, 2014; Blakey, 2021). Two periods during the Mesozoic, i.e. the late Jurassic and the middle Triassic are characterized by deposition of organic-rich marine muds on the circum-arctic continental margins (Leith et al., 1993; Stein, 2007; Moore et al., 2011). The late Jurassic is represented by the Upper Kingak Formation on the Alaska North Slope, the Husky Formation on the McKenzie Delta, the Ringnes Formation in the Sverdrup Basin and the Aagardfjellet Formation (Dybvik, 1985; Ohm et al., 2019; Weniger et al., 2019) in the Svalbard area. Examples of organic-rich middle Triassic muds are the Shublik Formation on the Alaska North Slope, the Murray Harbour and Hoyle Bay Formations in the Sverdrup Basin and the Botneheia Formation on Svalbard. The fluid escape pipes discovered on the Lomonosov Ridge thus represent the first indications of hydrocarbon source rocks present on the pre-Cenozoic continental margin of polar Europe.

7. Conclusions

Local seismic amplitude anomalies in the sediments 0.3–0.8 s (~240–500 m) sub-bottom are present at four separate locations in water depths of ~1200 m on top of the North American segment (89°N-85°N) of the Lomonosov Ridge. The acoustic sections across the sites show <1.5 km wide and <25 m high domes with a central pipe (width <600 m) of amplitude anomalies ranging from continuous to chaotic. These features are considered to represent sites of gas-charged fluid migration terminating at the seabed as a pock mark. The doming and pipe formation was generated by mobilization of unstable high porosity and low density Eocene bio-siliceous ooze triggered by intruding free gas and fluids from deeper pre-Cenozoic hydrocarbon source beds. The paleo-position of the pipes was the continental margin of a restricted Mesozoic polar basin, which experienced deposition of hydrocarbon source rocks during the late Jurassic and the middle Triassic.

Declaration of competing interest

The authors declare that they have no known competing financial interests or personal relationships that could have appeared to influence the work reported in this paper.

References

Akhmetiev, M.A., Zaporozhets, N.I., Benyamovskiy, V.N., Aleksandorva, G.N., Iakoleva, A.I., Oreshkina, T.V., 2012. The paleogene history of the western siberian seaway – a connection of the peri-tethys to the Arctic Ocean. Aust. J. Earth Sci. 105/1, 50–67.

Arntsen, B., Wensaas, L., Løseth, H., Hermanrud, C., 2007. Seismic modeling of gas chimneys. Geophys 72, 251–259.

Backman, J., Jakobsson, M., Frank, M., Sangiorgi, F., Brinkhuis, H., Stickley, C., O'Regan, M., Løvlie, R., Palike, H., Spofforth, J., Gattacecca, J., Moran, K., King, J., Heil, C., 2008. Age model and core-seismic integration for the cenozoic arctic coring expedition sediments from the Lomonosov Ridge. Paleoceanography 23, PA1S03. https://doi.org/10.1029/2007PA001476.

Barnett-Moore, N., Muller, D., Williams, S., Skogseid, J., Seton, M., 2016. A reconstruction of the north atlantic since the earliest jurassic. Basin Res. 30, 160–185. https://doi.org/10.1111/bre.12214.

Berndt, C., Bünz, S., Clayton, T., Mienert, J., Sanders, M., 2004. Seismic character of bottom simulating reflectors: examples from the mid-Norwegian margin. Mar. Petrol. Geol. 21, 723–733.

Bird, A.A., Weatherly, G.L., Wimbush, M., 1982. A study of the bottom boundary layer over the eastward scarp of the Bermuda Rise. J. Geophys. Res. 87, 7941–7954.

Bowden, K.F., 1960. The dynamics of flow on a submarine ridge. Tellus 12, 418–426.

Blakey, R., 2021. Paleotectonic and paleogeographic history of the Arctic region. Atl. Geol. 57 (1) https://doi.org/10.4138/atlgeol.2021.002, 007–039.

Borowski, W.S., Paull, C.K., Ussler, W., 1999. Global and local variations of interstitial sulfate gradients in deep-water, continental margin sediments: sensitivity to underlying methane and gas hydrates. Mar. Geol. 159, 131–154. https://doi.org/10.1016/S0025-3227(99)00004-3.

Brikiatis, L., 2014. The De Geer, Thulean and Beringia routes: key concepts for understanding early Cenozoic biogeography. J. Biogeogr. 41, 1036–1105.

Buchanan, K.L., Ernst, R.E., 2006. The high arctic large igneous Province (HALIP): evidence for an associated giant radiating dyke swarm. http://www.largeigneous provinces.org/06apr.

Campsie, J., Rasmussen, M.H., Hansen, N., Liebe, C.J., Laursen, J., Brochwicz-Levinski, W., Johnson, L., 1988. K-Ar ages of basaltic rocks collected during a traverse of the Franz Josef Land archipelago (1895- 1896). Polar Res. 6, 173–177.

Cartwright, J., Santamarina, C., 2015. Seismic characteristics of fluid escape pipes in sedimentary basins: implications for pipe genesis. Mar. Petrol. Geol. 65, 126–140.

Chernykh, A.A., Krylov, A.A., 2017. Duration, causes, and geodynamic significance of the Middle Cenozoic Hiatus in sedimentation in the near-polar part of the LR (based on IODP-302-ACEX drilling data). Oceanology 57 (5), 675–684. https://doi.org/10.1134/S0001437017050058.

Corfu, F., Polteau, S., Planke, S., Faleide, J.I., Svensen, H., Zayoncheck, A., Stolbov, N., 2013. U–Pb geochronology of cretaceous magmatism on svalbard and Franz Josef Land, barents sea large igneous Province. Geol. Mag. 150 (6), 1127–1135. https://doi.org/10.1017/S0016756813000162.

Dibner, V.D., 1978. Franz Josef Land sedimentary mega-plateau. In: Sokolov, V.N. (Ed.), Morpho-structure of the Barents Shelf. Proc. Sci. Res. Inst. Arctic Geology, vol. 185. Nedra, Leningrad, pp. 57–75.

Dibner, V.D., 1998. Geology of Franz Josef Land. Nor. Polarinst. Medd. 146, 190.

Drachev, S., Saunders, A.D., 2006. The Early Cretaceous Arctic LIP: its geodynamic setting and implications for Canada Basin opening. Proc. Int. Conf. Arctic Margins IV (Halifax, Nova Scotia, Canada).

Dybvik, H., 1985. Jurassic and cretaceous black shales of the janusfjellet formation, svalbard, Norway. Sediment. Geol. 41, 235–248.

Expedition 302 Scientists, 2006. Sites M0001-M0004. In: Backman, J., Moran, K., McInroy, D.B., Mayer, L.A., the (Eds.), Expedition 302 Scientists. Proc. IODP, vol. 302. https://doi.org/10.2204/iodp.proc.302.104.2006. College Station TX.

Gaina, C., Roest, W.R., Müller, R.D., 2002. Late cretaceous-cenozoic deformation of northeast asia. Earth Planet Sci. Lett. 197, 273–286.

Gakkel, Y.Y., 1958. Signs of recent submarine volcanic activity on the Lomonosov Range. Priroda 4, 90–97 (translated from Russian).

Gay, A., Mourgues, R., Berndt, C., Bureau, D., Planke, S., Laurent, D., Gautier, S., Lauer, C., Loggia, D., 2012. Anatomy of a fluid pipe in the Norway Basin: initiation, propagation and 3D shape. Mar. Geol. 332–334, 75–88.

Glebovsky, V.Yu, Kaminsky, V.D., Minakov, A.N., Merkur'ev, S.A., Childers, V.A., Brozena, J.M., 2006. Formation of the Eurasia Basin in the Arctic Ocean as inferred from geohistorical analysis of the anomalous magnetic field. Geotectonics 40 (4), 263–281.

Guerin, G., Goldberg, D., 2005. Modeling of acoustic wave dissipation in gas hydrate-bearing sediments. G-cubed 6 (7), 1–16. https://doi.org/10.1029/2005GC000918.

Gramberg, I., Kiselev, Yu G., Konovalov, V.V., 1991. Seismic studies from drift stations "North Pole". Soviet Geol. N3 45–54.

Hansen, J.P.V., Cartwright, J.A., Huuse, M., Clausen, O.R., 2005. 3D seismic expression of fluid migration and mud remobilization on the Gjallar Ridge, offshore mid-Norway. Basin Res. 17, 123–139.

Hansen, D.M., 2006. The morphology of intrusion-related vent structures and their implications for constraining the timing of intrusive events along the NE Atlantic margin. J. Geol. Soc., London 163, 789–800.

Hornbach, M.J., Holbrook, W.S., Gorman, A.R., Hackwith, K.L., Lizarraide, D., Pecher, I., 2003. Direct seismic detection of methane hydrate on the Blake Ridge. Geophys 68, 92–100.

Hovland, M., Talbot, M., Quale, H., Olaussen, S., Aasberg, L., 1987. Methane-related carbonate cements in pockmarks of the north sea. J. Sediment. Res. 57, 881–892. https://doi.org/10.1306/212F8C92-2B24-11D7-8648000102C1865D.

Hovland, M., Gardner, J., Judd, A.G., 2002. The significance of pockmarks to understanding fluid flow processes and geohazards. Geofluids 2, 127–136.

Hunkins, K., Thorndike, E.M., Mathieu, G., 1969. Nepheloid layer and bottom currents in the Arctic Ocean. J. Geophys. Res. 74, 6995–7007.

Hustoft, S., Bünz, S., Mienert, J., 2010. Three-dimensional seismic analysis of the morphology and spatial distribution of chimneys beneath the Nyegga pockmark field, offshore mid-Norway. Basin Res. 22, 465–480.

Huuse, M., Jackson, C., Van Rensbergen, P., Davies, R.J., Flemings, P.B., Dixon, R.J., 2010. Subsurface sediment remobilization and fluid flow in sedimentary basins: a review. Basin Res. 22, 342–360.

Jain, A.K., Juanes, R., 2009. Preferential Mode of gas invasion in sediments: grain-scale mechanistic model of coupled multiphase fluid flow and sediment mechanics. J. Geophys. Res. 114, B08101. https://doi.org/10.1029/2008JB006002.

Jakobsson, M., Mayer, L.A., Coakley, B., Dowdeswell, J.A., Forbes, S., Fridman, B., Hodnesdal, H., Noormets, R., Pedersen, R., Rebesco, M., Schenke, H.-W., Zarayskaya, Y., Accettella, A.D., Armstrong, A., Anderson, R.M., Bienhoff, P., Camerlenghi, A., Church, I., Edwards, M., Gardner, J.V., Hall, J.K., Hell, B., Hestvik, O.B., Kristoffersen, Y., Marcussen, C., Mohammad, R., Mosher, D., Nghiem, S.V., Pedrosa, M.T., Travaglini, P.G., Weatherall, P., 2012. The international bathymetric chart of the Arctic Ocean (IBCAO) version 3.0. Geophys. Res. Lett. 39 (12), L12609. https://doi.org/10.1029/2012gl052219.

Johnson, G.L., Heezen, B.C., 1967. The arctic mid-oceanic ridge. Nature 215, 724–725.

Jokat, W., Uenzelmann-Neben, G., Kristoffersen, Y., Rasmussen, T.M., 1992. Lomonosov Ridge – a double-sided continental margin. Geology 20, 887–890.

Jokat, W., 2005. The sedimentary structure of the Lomonosov Ridge between 88°N and 80°N. Geophys. J. Int. 163 (2), 698–726. https://doi.org/10.1111/j.1365246X.2005.02786.x.

Judd, A.G., Hovland, M., 2007. Seabed Fluid Flow – the Impact on Geology, Biology and the Marine Environment. Cambridge Univ. Press, Cambridge.

Judd, A., Noble-James, T., Golding, N., Eggett, A., Diesing, M., Clare, D., Silburn, B., Duncan, G., Field, L., Milodowski, A., 2020. The Croker Carbonate Slabs: extensive methane-derived authigenic carbonate in the Irish Sea—nature, origin, longevity and environmental significance. Geo Mar. Lett. 40, 423–438. https://doi.org/10.1007/s00367-019-00584-0.

Karasik, A.M., 1968. Magnetic anomalies of the gakkel Ridge and the origin of the Eurasia sub-basin of the Arctic Ocean. Geophysical methods of prospecting in the Arctic, NIIGA, Leningrad 5, 8–19 (translated from Russian).

Knudsen, C., Hopper, J.R., Bierman, P.R., Bjerager, M., Funck, M., Green, P.F., Ineson, J. R., Japsen, P., Marcussen, C., Sherlock, S.C., Thomsen, T.B., 2017. Samples from the Lomonosov Ridge place new constraints on the geological evolution of the Arctic Ocean. In: Pease, V., Coakley, B. (Eds.), Circum-Arctic Lithosphere Evolution, vol. 460. Geol. Soc., London, Special Publications. https://doi.org/10.1144/SP460.17.

Kristoffersen, Y., Mikkelsen, N., 2006. On sediment deposition and nature of the plate boundary at the junction between the submarine Lomonosov Ridge, Arctic Ocean and the continental margin of Arctic Canada/North Greenland. Mar. Geol. 225, 265–278.

Kravchishina, M.D., Lein, A., Flint, M.V., Baranov, B.V., Miroshnikov, A., Dubinina, E.O., Dara, O.M., Boev, A.G., Savvichev, A.S., 2021. Methane-derived authigenic carbonates on the seafloor of the laptev sea shelf. Front. Mar. Sci. https://doi.org/10.3389/fmars.2021.690304.

Kristoffersen, Y., Coakley, B.J., Hall, J.K., Edwards, M., 2007. Mass wasting on the submarine Lomonosov Ridge, central Arctic Ocean. Mar. Geol. 243, 132–142.

Kristoffersen, Y., Tholfsen, A., Hall, J.K., Stein, R., 2016. Scientists spend arctic winter adrift on sea ice. Eos, Trans. Am. Geophys. Union 97, 10.1029/2016EO060711. 11 October 2016.

Kristoffersen, Y., Hall, J.K., Harris Nilsen, E., 2021. Morris Jesup Spur and -Rise north of Greenland – exploring present seabed features, the history of sediment deposition, volcanism and tectonic deformation at a Late Cretaceous/early Cenozoic triple junction in the Arctic Ocean. Norw. J. Geol. 101, 202104. https://doi.org/10.17850/njg101-1-4.

Langinen, A.E., Lebedev-Ivanova, N.N., Gee, D.G., Zamansky, Yu Ya, 2009. Correlations between the Lomonosov Ridge, Marvin spur and the adjacent basins of the Arctic Ocean based on seismic data. Tectonophysics 72, 309–322.

Lee, M.W., Hutchinson, D.R., Dillon, W.P., Miller, J.J., Agena, W.F., Swift, B.A., 1993. A method of estimating the amount of in situ gas hydrates in deep marine sediments. Mar. Petrol. Geol. 10, 494–506.

Lee, M.W., Dillon, W., 2001. Amplitude blanking related to the pore-filling of gas hydrate in sediments. Mar. Gephys. Res. 22, 101–109.

Leith, T.L., Weiss, H.M., Mørk, A., Århus, N., Elvebakk, G., Embry, A., Brooks, P.W., Stewart, K.R., Pchelina, T.M., Brio, E.G., Verba, M.L., Danyushevskaya, A., Borisov, A.V., 1993. Mesozoic hydrocarbon source-rocks of the Arctic region. Norw. Pet. Soc. Special Publication 2, 1–25.

Løseth, H., Wensaas, L., Arntsen, B., Hanken, N., Basire, C., Graue, K., 2001. 1000 m long gas blow out pipes. In: 63rd EAEG Conference and Exhibition, Extended Abstracts, p. 524.

Løseth, H., Wensaas, L., Arntsen, B., Hovland, M., 2003. Gas and fluid injection triggering shallow mud mobilization in the Hordaland Group, North Sea. In: Van Rensbergen, P., Hillis, R.R., Maltman, A.J., Morley, C.K. (Eds.), Subsurface Sediment Mobilization, vol. 216. Geol. Soc., London, Special Publication, pp. 139–157.

Løseth, H., Gading, M., Wensaas, L., 2009. Hydrocarbon leakage interpreted on seismic data. Mar. Petrol. Geol. 26, 1304–1319.

Løseth, H., Wensaas, L., Arntsen, B., Hanken, N., Basire, C., Graue, K., 2011. 1000 m long gas blow out pipes. Mar. Petrol. Geol. 28, 1047–1060.

Madof, A., 2018. Gas hydrates in coarse-grained reservoirs interpreted from velocity pull-up: Mississippi Fan, Gulf of Mexico. Geology 46, 559–562.

Maestrelli, D., Iacopini, D., Jihad, A., Bond, C.E., Bonini, M., 2017. Seismic and structural characterization of fluid escape pipes using 3D and partial stack seismic from the Loyal Field: a multiphase and repeated intrusive mechanism. Mar. Petrol. Geol. 88, 489–510. https://doi.org/10.1016/j.marpetgeo.2017.08.

Magalhãesa, V.H., Pinheiro, L.M., Ivanov, M.K., Kozlova, E., Blinova, V., Kolganova, J., Vasconcelos, C., McKenzie, J.A., Bernasconi, S.M., Kopf, A.J., Díaz-del-Río, V., González, F.J., Somoza, L., 2012. Formation processes of methane-derived authigenic carbonates from the Gulf of Cadiz. Sediment. Geol. 243–244, 155–168. https://doi.org/10.1016/j.sedgeo.2011.10.013.

Malthe-Sørenssen, A., Planke, S., Svensen, H., Jamtveit, B., 2004. Formation of saucer-shaped sills. In: Breitkreuz, C., Petford, N. (Eds.), Physical Geology of High-Level Magmatic Systems, vol. 234. Geol. Soc., London, Special Publication, pp. 215–227.

Mann, U., Knies, J., Chans, S., Jokat, W., Stein, R., Zweigel, J., 2009. Modelling of tertiary source rocks in the central Arctic Ocean. Mar. Petrol. Geol. 26, 1624–1639.

McCave, I.N., Hall, I.R., Antia, A.N., Chou, L., Dehairs, F., Lampitt, R.S., Thomsen, L., van Weering, T., Wollast, R., 2001. Distribution, composition and flux of particulate material over the European margin at 47–50N. Deep-Sea Res. II 48, 3107–3139.

Moore, T.E., Grantz, A., Pitman, J.K., Brown, P., 2011. A first look at the petroleum geology of the Lomonosov Ridge microcontinent, Arctic Ocean. In: Spencer, A.M., Embry, A.F., Gautier, D.L., Stoupakova, A.V., Sørensen, K. (Eds.), Arctic Petroleum Geology, vol. 35. Geol. Soc., London, pp. 751–769. https://doi.org/10.1144/M35.49. Memoir.

Moran, K., Backman, J., Brinkhuis, H., Clemens, S., Cronin, T., Dickens, G., Eynaud, F., Gattacceca, J., Jakobsson, M., Jordan, R., Kaminski, M., King, J., Koc, N., Krylov, A., Martinez, N., Matthiessen, J., McInroy, D., Moore, T., Onodera, J., Jokat, W., Kristoffersen, Y., 2006. The cenozoic paleoenvironment of the Arctic Ocean. Nature 441, 601–605.

Morley, C.K., 2003. Outcrop examples of mudstone intrusions from the Jerudong anticline, Brunei Darussalam and inferences for hydrocarbon reservoirs. In: van Rensbergen, P., Hillis, R.R., Maltman, A.J., Morley, C.K. (Eds.), Susurface Sediment Mobilization, vol. 216. Geol. Soc., London, Special Publications, pp. 381–394.

Moss, J.L., Cartwright, J., 2010. 3D seismic expression of km-scale fluid escape pipes from offshore Namibia. Basin Res. 22, 481–501.

Nørgaard-Pedersen, N., Mikkelsen, N., Kristoffersen, Y., 2007. Arctic Ocean record of last two glacial-interglacial cycles off North Greenland/Ellesmere Island—implications for glacial history. Mar. Geol. 244, 93–108.

Ogawa, Y., Takahashi, K., Yamanaka, T., 2008. Paleoceanography of the middle Eocene Arctic Ocean based on geochemical measurements of biogenic matter. Memoir. Facul. Sci. Kyushu Univ. Earth Planet. Sci. XXXII (1), 31–48.

Ohm, S.E., Larsen, L., Olaussen, S., Senger, K., Birchall, T., Demchuk, T., Hodson, A., Johansen, I., Titlestad, G.O., Karlsen, D.A., Braathen, A., 2019. Discovery of shale gas in organic-rich jurassic successions, adventdalen, central spitsbergen, Norway. Norw. J. Geol. 99, 349–376. https://doi.org/10.17850/njg007.

O'Regan, M., King, J., Backman, J., Jakobsson, M., Pälike, H., Moran, K., Heil, C., Sakamoto, T., Cronin, T., Jordan, R.W., 2008. Constraints on the Pleistocene chronology of sediments from the Lomonosov Ridge. Paleoceanography 23, PA1S19. https://doi.org/10.1029/2007PA001551.

O'Regan, M., Moran, K., 2010. Deep water methane hydrates in the Arctic Ocean: reassessing the significance of a shallow BSR on the Lomonosov Ridge. J. Geophys. Res. 115, B05102. https://doi.org/10.1029/2009JB006820.

O'Regan, M., Moran, K., Baxter, C.D., Cartwright, J., Vogt, C., Kolling, M., 2010. Towards ground truthing exploration in the central Arctic Ocean: a Cenozoic compaction history from the Lomonosov Ridge. Basin Res. 22 (2), 215–235. https://doi.org/10.1111/j.1365-2117.2009.00403.x.

Ostenso, N.A., Wold, R.J., 1977. A seismic and gravity profile across the Arctic Ocean Basin. Tectonophysics 37, 1–24.

Piepjohn, K., von Gosen, W., Tessensohn, F., 2016. The Eurekan deformation in the Arctic: an outline. J. Geol. Soc. https://doi.org/10.1144/jgs2016-081. London.

Plaza-Faverola, A., Westbrook, G.K., Ker, S., Exley, R.J.K., Gailler, A., Minshull, T.A., Broto, K., 2010. Evidence from three-dimensional seismic tomography for a substantial accumulation of gas hydrate in a fluid-escape chimney in the Nyegga pockmark field, offshore Norway. J. Geophys. Res. 115, B08104. https://doi.org/10.1029/2009JB007078.

Poirier, A., Hillaire-Marcel, C., 2011. Improved Os-isotope stratigraphy of the Arctic Ocean. Geophys. Res. Lett. 38, L14607, 1029/2011L047953.

Polyak, L., Jakobsson, M., 2011. Quaternary sedimentation in the Arctic Ocean: recent advances and further challenges. Oceanography 24, 53–64.

Planke, S., Rasmussen, T., Rey, S.S., Myklebust, R., 2005. Seismic characteristics and distribution of volcanic intrusions and hydrothermal vent complexes in the Vøring and Møre basins. In: Doré, A.G., Vinin, G.B.A. (Eds.), Petroleum Geology: North-West Europe and Global Perspectives—Proc. 6th Pet. Geol. Conf. Geol. Soc., London, pp. 833–844.

Rekant, P., Sobolev, N., Portnov, A., Belyatsky, B., Direp, G., Pakhalko, A., Kaban`kov, V., Andreeva, I., 2019. Basement segmentation and tectonic structure of the Lomonosov Ridge, Arctic Ocean: insights from bedrock geochronology. J. Geodyn. 128, 38–54.

Rigor, I.G., Wallace, J.M., Colony, R.L., 2002. Response of sea ice to the arctic oscillation. J. Clim. 15, 2648–2668.

Rudels, B., Friedrich, H., Quadfasel, D., 1999. The arctic circum-polar boundary current. Deep-Sea Res. 46, 1023–1062.

Sauermilch, I., Weigelt, E., Jokat, W., 2018. Pre-rift sedimentation of the Lomonosov Ridge, Arctic Ocean at 84°N—a correlation to the complex geologic evolution of the conjugated kara sea. J. Geodyn. 118, 49–54. https://doi.org/10.1016/j.jog.2018.05.002.

Schroder-Adams, C., 2013. The Cretaceous Polar and Western Interior seas: paleoenvironmental history and palaeoceanographic linkages. Sediment. Geol. 301, 26–40.

Shipboard Scientific Party, 2005. Arctic coring expedition (ACEX): palaeoceanographic and tectonic evolution of the central Arctic Ocean. IODP Preliminary Report 302. http://iodp.tamu.edu/publications/PR/302PR/302PR.PDF.

Shipilov, E.-V., 2016. Basalt magmatism and strike-slip tectonics in the Arctic margin of Eurasia: evidence for the early stage of geodynamic evolution of the Amerasia Basin. Russ. Geol. Geophys. 57, 1668–1687.

Shipley, T.H., Houston, M.H., Buffler, R., Shaub, J., McMillen, K.J., Ladd, J., Worzel, J.L., 1979. Seismic evidence for widespread possible gas hydrate horizons on continental slopes and rises. Am. Assoc. Petrol. Geol. Bull. 63, 2204–2213.

Sellén, E., Jakobsson, M., Backman, J., 2008. Sedimentary regimes in arctic's amerasian and eurasian basins: clues to differences in sedimentation rates. Global Planet. Change 61, 275–284.

Stein, R., Boucsein, B., Meyer, H., 2006. Anoxia and high primary production in the Paleogene central Arctic Ocean: first detailed records from Lomonosov Ridge. Geophys. Res. Lett. 33, L18606. https://doi.org/10.1029/2006GL026776.

Stein, R., 2007. Upper Cretaceous/Lower Tertiary black shales near the North Pole: organic- carbon origin and source rock potential. Mar. Petrol. Geol. 24, 67–73.

Svensen, H., Planke, S., Jamtveit, B., Pedersen, T., 2003. Seep carbonate formation controlled by hydrothermal vent complexes: a case study from the Vøring Basin, the Norwegian Sea. Geo Mar. Lett. 23, 351–358.

Vogt, P.R., Taylor, P.T., Kovacs, L.C., Johnson, G.L., 1979. Detailed aeromagnetic investigation of the arctic basin. J. Geophys. Res. 84, 1071–1089.

Weigelt, E., Jokat, W., Eisermann, H., 2020. Deposition history and paleo-current activity on the southeastern Lomonosov Ridge and its Eurasian flank based on seismic data. G-cubed 21. https://doi.org/10.1029/2020GC009133 e2020GC009133.

Weniger, P., Blumenberg, M., Berglar, K., Ehrhardt, A., Klitzke, P., Krüger, M., Lütz, R., 2019. Origin of near-surface hydrocarbon gases bound in northern Barents Sea sediments. Mar. Petrol. Geol. 102, 455–476.

Westbrook, G.K., Exley, R., Minshull, T.A., Nouzé, H., Gailler, A., Jose, T., Ker, S., Plaza-Faverola, 2008. High-resolution 3-D seismic investigations of hydrate-bearing fluid-escape chimneys in the Nyegga region of the Vøring Plateau, Norway. In: Proceedings of the 6th International Conference on Gas Hydrates (ICGH 2008). Vancouver, BC, Canada. https://circle.ubc.ca/handle/2429/1022.

Wilson, J.T., 1963. Hypothesis of earth's behavior. Nature 198, 925–929.

Xu, W., Ruppel, C., 1999. Predicting the occurrence, distribution, and evolution of methane gas hydrate in porous marine sediments. J. Geophy. Res. 104 (B3), 5081–5095.

Zakharov, Y.D., Shigeta, Y., Popov, A.M., Velivetskaya, T.A., Afanasyeva, T.B., 2011. Cretaceous climatic oscillations in the Bering area (Alaska and Koryak Upland): isotopic and paleontological evidence. Sediment. Geol. 235, 122–131.

Zatsepina, O., Buffett, B., 1997. Phase equilibrium of gas hydrates: implications for the formation of hydrate in the deep-sea floor. Geophys. Res. Lett. 24, 1567–1570.